JAERI-Review
98-002

STUDIES OF HIGH-LEVEL WASTE FORM PERFORMANCE AT JAPAN ATOMIC ENERGY RESEARCH INSTITUTE

February 1998

Tsunetaka BANBA, Hisayoshi MITAMURA, Kenichi KURAMOTO,
Yahohiro INAGAKI* and Hiroshi KAMIZONO

日本原子力研究所
Japan Atomic Energy Research Institute

本レポートは，日本原子力研究所が不定期に公刊している研究報告書です。
入手の問合わせは，日本原子力研究所研究情報部研究情報課（〒319-1195 茨城県那珂郡東海村）あて，お申し越しください。なお，このほかに財団法人原子力弘済会資料センター（〒319-1195 茨城県那珂郡東海村日本原子力研究所内）で複写による実費領布をおこなっております。

This report is issued irregularly.
Inquiries about availability of the reports should be addressed to Research Information Division, Department of Intellectual Resources, Japan Atomic Energy Research Institute, Tokai-mura, Naka-gun, Ibarakiken 319-1195, Japan.

編集兼発行　日本原子力研究所
印　　刷　ニッセイエブロ株式会社

Studies of High-Level Waste Form Performance at Japan Atomic Energy Research Institute

Tsunetaka BANBA, Hisayoshi MITAMURA, Kenichi KURAMOTO, Yahohiro INAGAKI* and Hiroshi KAMIZONO

Department of Environmental Safety Research
Nuclear Safety Research Center
Tokai Research Establishment
Japan Atomic Energy Research Institute
Tokai-mura, Naka-gun, Ibaraki-ken

(Received January 9, 1998)

The JAERI studies on the properties of the glass and ceramic waste forms, which have been done in the last several years, are described briefly. For the long-term evaluation of glass waste form performance under repository condition, leachability has studied from the standpoints of understanding of alteration layers, effects of groundwater and effects of redox condition using the radioactive or non-radioactive glass samples. The studies revealed that (1) the reactions in the alteration layers, such as crystal growth, continue after the apparent release of elements from the glass almost ceases, (2) under somewhat reducing conditions, Fe dissolves easily into leachates, and hydrated silicate surface layer tends to dissolve more easily with Fe in reduced synthetic groundwater than in deionized water, (3) precipitation of $PuO_2 \cdot xH_2O$(am) is controlling the leaching of soluble species of Pu under both redox conditions, and the dominant soluble species is $Pu(OH)_4^0$ under reducing condition. Ceramics are considered as most promising materials for the actinide-rich wastes arising from partitioning and transmutation processes because of their outstanding durability for long term. In the present study, α-decay damage effects on the density and leaching behavior of perovskite (one of three main minerals forming Synroc) were investigated by an accelerated experiment using the actinide doping technique. A decrease in density of Cm-doped perovskite reaches 1.3 % at a dose of 9×10^{17} α-decays$\cdot g^{-1}$. The leach rate of perovskite increases with an increase in accumulated α-decay doses. Application of zirconia- and alumina-based ceramics for incorporating actinides was also investigated by inactive laboratory tests with an emphasis on crystallographic phase stability and chemical durability. The yttria-stabilized zirconia is stable crystallographically in the wide ranges of Ce and/or Nd content and have excellent chemical durability.

Keywords: Glass Waste Form, Ceramic Waste Form, Leachability, Repository Condition, Synroc, α-Decay Damage, Yttria-stabilized Zirconia

---

This report was prepared for the fourth research coordination meeting of IAEA Coordinated Research Programme (CRP) on "Performance of High-Level Waste Forms and Packages under Repository Conditions", which was held in Marcoule, France, from 14 to 18 April 1997.

* Kyushu University

原研における高レベル放射性廃棄物固化体に関する研究

日本原子力研究所東海研究所安全性試験研究センター環境安全研究部
馬場　恒孝・三田村久吉・蔵本　賢一・稲垣八穂広*・上薗　裕史

（1998年1月9日受理）

ガラス及びセラミック固化体の特性に関する最近の原研の研究成果を簡単に紹介する。処分条件下でのガラス固化体の長期性能評価を目的として、その浸出挙動を変質層の役割、地下水による影響及び酸化還元雰囲気の影響の観点から研究を進めた。その結果、次のことが明らかになった。①浸出の過程で表面に形成した変質層内での結晶成長のような反応は、固化体からの元素の浸出がほとんど止まっても進行する。②水和したケイ酸変質層は、脱イオン水中よりも還元性の合成地下水中の方でFeを伴って溶解し易い傾向がある。③酸化還元両条件ともに$Pu_2xH_2O(am)$の形成がPuの浸出を支配し、還元条件下での主な可溶性化学種は$Pu(OH)_4^0$である。

セラミック固化体に関する研究では、シンロックの構成鉱物の１つであるペロブスカイトのα崩壊損傷を調べ、$9x10^{17}\ \alpha/g$の蓄積線量で1.3%の密度減少を観察した。また、ペロブスカイトの浸出率は蓄積線量の増加で増える傾向のあることが分かった。さらに、群分離したTRU核種の固化用に検討しているジルコニア及びアルミナを主成分とするセラミックの結晶学的安定性、化学的耐久性等をCe及びNdを用いて調べた。その結果、イットリア安定化ジルコニアが目的とする固化体として優れた特性を有することが明らかになった。

東海研究所：〒319-1195　茨城県那珂郡東海村白方白根２－４
本報告書の内容は1997年4月、フランスのマルクールで開催されたIAEA協力研究計画(CRP)「処分条件下の高レベル廃棄物固化体及び固化体容器の性能に関する第4回研究調整会議」で報告したものである。
＊ 九州大学

Contents

目　　次

This is a blank page.

1. INTRODUCTION

The Japan Atomic Energy Research Institute (JAERI) has contributed to the establishment of the national system for the high-level radioactive waste management with developments of safety assessment methods and accumulation of useful data. Besides, JAERI is responsible for researches of new technology to be acceptable to the Japanese environmental circumstances.

In the present report, the JAERI studies on the properties of glass waste forms and ceramic waste forms, which have been done in the last several years, are described briefly.

2. GLASS WASTE FORMS

2.1 Growth Rate of Alteration Layer and Elemental Mass Losses during Leaching of Nuclear Waste Glass [1]

In order to validate the predictive models of the long-term corrosion of nuclear waste forms, the concept of natural analogues has been proposed [2]. The problem is, however, how we utilize the information of the natural analogues for modelling. One of the ways is to justify confidence in the theoretical model by correctly predicting the phases formed in the alteration layers of naturally and experimentally altered glasses. That is why a detailed understanding of the mineralogy and geochemistry of the layers is required [3]. In the present work, we will discuss on the growth rates of the alteration layers of a borosilicate nuclear waste glass and their relevance to elemental mass losses.

Experimental

MCC-1 leaching tests [4] were carried out for a borosilicate waste glass (Table 1) in deionized water for up to 364 days at 90°C. Four platy samples (0.2 x 0.5 x 0.5 cm) were put into a Teflon container for each leaching period. The surface area to solution volume ratio was 0.1 cm^{-1}. One of the four samples was immersed in ethanol for 2 hrs immediately after removing it from the leachate to prevent the shrinkage of the alteration layer during drying. The other samples were air-dried. Low viscosity epoxy resin was poured onto the ethanol-immersed sample when the ethanol was discarded. The air-dried samples were vacuum impregnated in the resin. After the polymerization of the resin, the samples were cut perpendicularly to the original glass surface and polished. The sections were subjected to optical microscopy (OM) in order to measure the layer thicknesses. When the layers were too thin for OM, the samples were cut by ultramicrotomy, creating sections 50 to 80 nm thick, and then subjected to analytical electron microscopy (AEM). The sections were also observed by scanning electron microscopy (SEM) for texture examination. The concentrations of the major elements in the alteration layers were measured by electron microprobe analysis (EMPA). Fine structures and mass fractions of the alteration layers were examined by AEM. The solution pH was measured after leaching and the elemental concentrations of the leachates were measured by inductively coupled plasma atomic emission spectroscopy (ICP-AES) or atomic absorption spectrometry (AAS).

Results and discussion

There is a sharp change in the layer growth of the leaching experiments before and after 91 days (Fig. 1). The thickness of the layer increases linearly at a rate of 0.63 μm/day for up to 91 days. However, in the 91 to 364-day period, the thickness remains constant (about 60 μm). This suggests that significant corrosion of the glass almost ceases after the 91-day leaching. Grambow et al. [5] pointed out that on the basis of the time dependence of palagonite rind development, the range of values for the forward rate is 3-20 μm/1000yrs and the value for the final rate is 0.1 μm/1000yrs at about 3°C. The layer growth before the 91-day leaching corresponds to the corrosion

of the forward reaction and the layer growth after the 91-day leaching, to the corrosion of the final reaction [6]. This is in good agreement with Si release data discussed below. We applied the relationship of the rates obtained by Grambow et al. [5] to our thickness measurements to calculate a corrosion rate of the final reaction of the waste glass. We assumed that the activation energy of the final reaction is the same as that of the forward reaction calculated from 3-20 μm/yrs (3°C) and 0.63 μm/day (90°C), i.e. 89-107 kJ/mole. A range of values of 0.003-0.03 μm/day was obtained for the final rate. The layer thickness may increase by 0.9-9 μm for 300 days in the final reaction, which explains the small change in the thickness after the 91-day leaching (Fig. 1).

Figure 2 shows the normalized elemental mass losses of some typical elements. The apparent releases of B, Na and Si cease in the 91 to 364-day leaching period. The NLs of Na and Si are lower than that of B because Na and Si still remain in the layers (Table 3). Because the increase in layer thickness ceases after the 91-day leaching, B, Na, and Si are not supplied from the glass. It is reasonable to suggest that there is no significant interactions, involving the three elements after 91 days.

The time dependence curves of B, Na and Si were similar to that of the layer thickness (Figs. 1 and 2), suggesting that the releases of these elements with time are related to the growth rate of the layer thickness. Because B can be completely depleted from the layer [7], the amounts of B in the leachates were used to calculate the layer thickness. The calculated values of layer thickness, represented by the triangles in Fig.1, agreed well with the observed values from the OM or AEM measurements. It is thus confirmed that the alteration layer thickness can be estimated by the amounts of B released. The agreement also implies that the shrinkage of the alteration layers during air-drying is not significant.

The small shrinkage was also confirmed by comparing the thicknesses of the ethanol-immersed layers with those of the air-dried layers. The comparison has revealed that the air-dried layers had almost the same thicknesses as those of the ethanol-immersed layers in the 1 to 91-day leaching period, but were thinner by around 5 percent in the 91 to 364-day period (Fig. 1); the air-dried layers had larger variabilities in the thicknesses.

The small shrinkage suggests that the progressive change in the Fe mass fractions from 5.2 % in the glass/layer interface to 20.1 % in the layer/solution interface [3] does not result from shrinkage but from a real relative increase in the Fe fraction owing to the depletion of some elements such as Na, B and Si. This means that the layers are progressively more porous towards the layer/solution interface. The selected EMPA analyses (Table 3) also suggest the porous structure of the layer. For instance, in the outermost of the layer where crystalline fibers are scattered in the amorphous matrix [3], 70 % of the original glass network formers are depleted (see the concentrations of B and Si in Tables 1 and 3). Thus, the alteration layer retains its structure despite the depletion of the large part of the glass network formers and the recrystallization. Naturally altered basaltic glasses are usually dried when they are obtained. It is not yet known whether the natural basaltic glass layers retain the structure of the layers after air-drying. The structural change of both naturally and experimentally altered layers during air-drying should be investigated.

The AEM studies revealed that new crystals have been formed in the 91-day experiment sample. The new crystals are texturally and chemically different from the fibers which are formed on the top of the layer [3]. The new crystals are distributed on the top of the fibers, and form a zonal structure like that of the fibers (Fig. 3). Both zones of the new crystals and fibers are parallel to the pristine glass surface. The thicknesses of the fiber zone (denoted as 2 in Fig. 3a) are 120, 130, 120, and 220 nm in the 14, 28, 91, and 364-day experiment, respectively. Thus, the thicknesses of the fiber zone remain almost constant during the 91-day leaching of the glass. The fact that the fiber zone grows in the 91 to 364-day leaching period indicates that "the reaction at the final rate" [6] still continues. The thicknesses of the zone of the new crystals (denoted as 3 in Fig. 3a) are 440 and 480 nm in the 91 and 364-day experiments, respectively. The mass fractions of the fibers and mottled phase in the 364-day experiment (Table 2) have similar characteristics to those observed in the 14-day experiment [3]; rich in Fe, Mn, Co, and Ni, and none of the rare earth elements or

Zr for the fibers, and rich in Fe, Zr, and the rare earth elements, and low in Co and Ni for the mottled phase. There appeared to be little change in the texture of the fibers and mottled phase near the layer/solution interface (Fig. 3a) The new crystals are characterized by the larger size (about 400 nm long), the consistent crystallographic orientation to the layer/solution interface (Fig. 3b), the d-spacing of 1.4 nm, and little Fe and enhanced Si (Table 2). These characteristics suggest that the new crystals are possibly smectite and therefore, mineralogically similar to the fibers. The mineralogical relationship between the new crystals and fibers is still under investigation. However, the thicknesses of the zones of the new crystals and fibers imply that the fibers grow while the new crystals do not and vice versa (e.g., 130 to 120 nm for the fiber zone and 0 to 440 nm for the new crystal zone in the 28 to 91-day leaching period).

The amount of Fe released in the solution is so small (Fig. 2) that it may be affected by the formation of minerals in the layer when Fe is not supplied from the glass, i.e., the layer thickness is almost constant. The growth of the fibers, which contain 10-18 % of Fe (Table 2, and Table II of ref. [3]), and the new crystals, which contain little Fe (Table 2), may account for the release of Fe in the solution: a slight decrease in the Fe release corresponds to the growth of the fibers and the non-growth of the new crystals in the 91 to 364-day leaching period.

Pit formation below the alteration layers was observed by OM and SEM on the samples leached for 91 to 364 days. Although the layer thickness ceased to increase, the degree of pitting increased with increase in the duration of the test. The cone-shaped pits (a few microns wide) are located inward from the glass-layer interface (Fig. 4). The loss of Na in the pit (number 2 in Table 3) indicates that the pits have been formed by the corrosion. The composition of the pit is similar to that of the layer near the glass/layer interface (number 3 in Table 3). Harker and Flintoff have also observed similar pit formation and attributed the pitting phenomena to the physical structure in the glass such as stress lines, surface roughening and microcracks [8]. It is almost certain that the point of origin of every pit may be at a center of physical weakness such as microcracks. However, because the pits were not observed during the first 56 days of leaching, the pitting phenomena may be strongly dependent on the local chemistry of leach solution such as pH. Analogous phenomena were observed for naturally altered basaltic glasses by Melson and Thompson [9]. Pits, which they called microtubules, are a few microns wide and filled by clay minerals like smectite. Clay minerals formed following a 364-day leaching experiment have not yet been found in pits.

2.2 Leaching Behavior of High-Level Waste Glass in Synthetic Groundwater [10,11]

The characteristics of groundwater affect leaching behavior of high-level waste glass, for example pH and Eh values may determine the precipitation processes of some elements in water. In the reduced synthetic groundwater which contains carbonate and sulfate ions, simulated high-level waste glass was subjected to static leach tests at 70° ± 1° and 20° ± 5°C. The glass-surface-area to leachant-volume ratio (SA/V ratio) was 0.24 cm^{-1} at 70°C and 0.12 cm^{-1} at 20°C. The static leach test at 70°C for up to 49 days was carried out in order to observe the process quickly. The static leach test at 20°C for 1 year was carried out for comparison with a former in-situ leach tests in one type of Japanese natural groundwater at 14°C. The four kinds of synthetic groundwater listed in Table 4 were used as leachants instead of the natural groundwater. Deionized water with a pH value of 5.6 and a specific resistance of 10^7 ohm cm was used as a reference.

Among normalized elemental mass losses (NL values) for the six elements, i.e., B, Si, Al, Fe, Nd and Ba, the value of NL_B was highest without exception, and the value of NL_{Ba} was lowest in some cases. The variation of NL_{Fe} is of particular interest, since it tended to be low in the case of deionized water and it was as high as NL_B in the case of synthetic groundwater Nos.1 to 3 at 20°C. The ratio of NL_{Fe}/NL_B is

introduced as an index expressing the extent of congruence. Table 5 summarizes the ratios of NL_{Fe}/NL_B under the present experimental conditions. The results in Table 5 can be interpreted in two ways. First, the ratio in synthetic groundwater tends to be higher than that in deionized water for each temperature and time condition, which means that in synthetic groundwater iron tends to dissolve more congruently and not to precipitate on the glass surface during leaching. Second, when the kind of water is fixed, the ratios of NL_{Fe}/NL_B are ordered as:

(20°C, 1 year) > (70°C, 28 days) > (70°C, 49 days)

with the exception of synthetic groundwater No.4 where a slight variation occurs.

Grooves were observed on the surface of the specimens leached in synthetic groundwater Nos.1 to 4. However, they were not clearly observed on the specimen leached in deionized water. It is thought that the grooves are clear in synthetic groundwater Nos.1 to 4 when congruent leaching tends to occur and not clear in deionized water when incongruent leaching occurs. Such grooves were also observed on the surface of the specimens leached in natural groundwater.

In synthetic groundwater Nos.1 to 4 which are reduced by tris-(hydroxymethyl)-aminomethane (THAM), the amount of Fe in the leachates increases as the Si increases probably as a result of the formation of $FeSiO_3$ colloidal particles or $FeSi_3O_3(OH)_8$ complex. It is not true that Fe very quickly reaches its saturation limit in synthetic groundwater Nos.1 to 4, since the formation of the colloids or complex will increase the solubility of Fe in leachates. Because the filtration of the leachate at 20°C for 1 year through a 0.025 μm membrane had almost no effect on the concentrations of Fe and Si, $FeSiO_3$ colloidal particles, if present, have a diameter of less than 0.025 μm.

In deionized water in an oxidized condition, NL_{Fe}/NL_B was smaller than that of synthetic groundwater, but this is not because of the higher pH values of the leachates. For example, in deionized water at 20°C the pH value was 7.3 and smaller than that in synthetic groundwater. Even in deionized water, there is at least one example in which the solution concentration of Fe does not decrease as the pH value increases. This example was observed with leach experiments at a high SA/V ratio of 0.85 cm^{-1}.

The role of THAM should be mentioned here. It tends to increase the pH and to decrease the Eh of the solution. The pH values of the present synthetic groundwater were adjusted to 7.7 (Table 4), and for this purpose about 5 g of THAM were used for a 1 liter solution. The use of THAM is thought to be a major cause for the congruent dissolution of the glass in synthetic groundwater Nos.1 to 4, since a Eh decrease by THAM in leachants will work effectively to form $FeSiO_3$ colloids or $FeSi_3O_3(OH)_8$ complex. As temperature rises and as time proceeds, THAM as a reducing agent will be consumed with the progress of leaching, resulting in a lower NL_{Fe}/NL_B ratio.

In conclusion, the examination of the leaching behavior of high-level waste glass in synthetic groundwater is quite useful for identifying and understanding the mechanisms involved. Under somewhat reducing conditions, Fe dissolves easily into leachates, and hydrated silicate surface layer on the glass surface tends to dissolve more easily with Fe in reduced synthetic groundwater than in deionized water. In synthetic groundwater, cracks originally present on the glass tend to open and are observed as evidence of congruent glass corrosion. It is speculated that, in deep geologic disposal sites, congruent dissolution is more likely to occur in an reducing environment with a high SA/V-ratio.

2.3 Effects of Redox Condition of Water on Pu and Cm Leaching from Waste Glass [12]

Most of actinides contained in the waste glasses are redox active, and their oxidation states, chemical species and equilibrium solubilities are greatly influenced by redox conditions. Therefore, the leaching behavior of actinides is expected to be greatly affected by redox conditions of water. The purpose of this study is to understand the effects of redox conditions of water on leaching behavior of actinides from the waste glass. Static corrosion tests were performed on the simulated waste glass doped with

Pu and Cm in deionized water at 90 °C with S/V ratio of 2600 m^{-1} under oxidizing and reducing conditions, respectively. Comparing the experimental results with thermodynamic data from other studies, the mechanism of the Pu and Cm leaching under reducing conditions are discussed.

Experimental

A powdered simulated waste glass doped with Pu and Cm ($^{238}PuO_2$; 0.06wt%, $^{240}PuO_2$; 0.16wt%,$^{244}Cm_2O_3$; 0.09wt%) was used as glass specimen. The grain size of the glass specimen was from 75 μm to 150 μm, and the specific surface area was 0.083m^2/g measured by BET method. Static corrosion tests on the glass specimen were performed in deionized water at 90°C under oxidizing and reducing conditions, respectively. The tests were performed in air for oxidizing conditions and in an airtight stainless steel container purged with mixed gas (Ar+5%H_2) as shown in Fig.5 for reducing conditions. The glass specimen (0.8g) and deionized water(25ml) were placed in a Teflon container with SA/V ratio of 2600m^{-1} and kept in a heating furnace at 90°C for periods of up to 92 days. The pH and Eh of the initial solution in air were measured to be 5.6 and +0.50V vs SHE at 25°C, respectively. While, the pH and Eh of the reducing solution were 6.9 and -0.35V vs SHE at 25°C, respectively.

After the corrosion tests, the Teflon container was cooled to room temperature, and the solution pH and Eh were measured immediately. The solution was filtered through 450nm and 1.8nm filters in order to investigate the distribution of the Pu and Cm particle size fractions, and the solution concentrations of Pu, Cm and other glass constituents were measured by a-spectrometry and ICP-AES.

Results

Figure 6 shows the solution pH and Eh as a function of corrosion time. It can be seen that the solution Eh under reducing conditions was maintained at approximately -0.45V vs SHE during the corrosion tests. While, the solution pH under both redox conditions decreased slowly with corrosion time after the rapid increase to the pH of 9.5 in a few days, which is expected to be due to the effects of radiolysis of water and gas.

The solution concentrations of major glass constituents are listed in Table 6, and Fig.7 shows the normalized concentrations(NC_i) as a function of corrosion time calculated by the following equation[13],

$$NC_i = C_i / f_i, \qquad (1)$$

where, C_i is the solution concentration of element i, and f_i is the original fraction of element i in the glass. It can be seen that redox conditions have no remarkable influence on the leaching of major glass constituents. Under both redox conditions, the effects of filtration on the solution concentrations were sufficiently small for Si and soluble elements(B, Li, Na, Mo). While, the effects of filtration were relatively large for Al and Ca, and the concentrations of Al and Ca in 1.8nm filtrates were thirty or forty percent of magnitude lower than those in non-filtered solutions.

The solution concentrations of Pu and Cm are listed in Table 7, and Fig.8 shows the concentrations as a function of corrosion time. It can be seen that redox conditions also have no remarkable influence on the leaching of Pu and Cm. Under both redox conditions, the effects of filtration were large, and the Pu and Cm concentrations in the 1.8nm filtrates were one or two orders of magnitude lower than those in the 450nm filtrates. While, there was no difference in the Pu and Cm concentrations between non-filtered solutions and 450nm filtrates.

Discussion

The present results showed that the redox conditions have no remarkable influence on the leaching behavior of Pu and Cm, which suggests that dominant oxidation states of the Pu and Cm in the solution under reducing conditions are the same as those under

oxidizing conditions. It was also observed that the Pu and Cm concentrations in the 1.8nm filtrates are one or two orders of magnitude lower than those in the 450nm filtrates under both redox conditions. The Pu and Cm concentrations in the 1.8nm filtrates are assumed to correspond to the soluble species controlled by the solubilities, and the difference in Pu and Cm concentrations between the 1.8nm and 450nm filtrates is assumed to correspond to the insoluble suspended fractions(colloidal particles). Therefore, it is suggested that the colloidal particles with the size from 1.8nm to 450nm are dominant phase for Pu and Cm in the solution under both redox conditions. On the other hand, NC_i for Pu and Cm are calculated to be $30g/m^3$ and $13g/m^3$ at the maximum, respectively. These values of NC_i for Pu and Cm are less than a tenth of the value for Si, which suggests that most of the Pu and Cm remains at the glass surface as the secondary phases under both redox conditions. Similar results of the leaching of actinides can be found in other corrosion tests performed under oxidizing and weakly reducing conditions[14,15,16].

Solubility of Pu in neutral aqueous solutions has been investigated by many researchers, and some thermodynamic data have been reported[17-22]. Comparing the present data on the Pu concentrations with the solubilities calculated by the thermodynamic data, reactions controlling the Pu leaching from glass can be estimated. On the other hand, only a few investigations are known on the solubility of Cm, and the comparison has not been done in the present study. For calculating the Pu solubility, the oxidation states of Pu must be evaluated. From the data of potentials for redox reactions[18], dominant oxidation states of Pu under the present oxidizing conditions (pH=8.8, Eh=+0.25V vs SHE) are expected to be Pu(IV), Pu(V) or Pu(VI), while the dominant oxidation states under the reducing conditions(pH=8.6, Eh=-0.45V vs SHE) are expected to be Pu(III) or Pu(IV). However, the present results showed that redox conditions have no influence on the solution concentrations of Pu($\sim 10^{-8}$M in the 1.8nm filtrates), which suggests that Pu(IV) is the dominant oxidation state in the solution under both redox conditions. The most feasible reaction controlling the solubility of Pu(IV) under the present conditions[15] is,

$$PuO_2 \cdot xH_2O(am) \leftrightarrow Pu^{4+} + 4OH^- + (x-2)H_2O, \quad \log K=-56.85[19]. \qquad (2)$$

In the solution, Pu^{4+} can make the complexation legands described as follows,

$$Pu^{4+} + OH^- \leftrightarrow Pu(OH)_3^+, \quad \log\beta=13.67[21], \qquad (3)$$
$$Pu^{4+} + 2OH^- \leftrightarrow Pu(OH)_2^{2+}, \quad \log\beta=28.20[21], \qquad (4)$$
$$Pu^{4+} + 3OH^- \leftrightarrow Pu(OH)_3^+, \quad \log\beta=38.85[21], \qquad (5)$$
$$Pu^{4+} + 4OH^- \leftrightarrow Pu(OH)_4^0, \quad \log\beta=49.20[21], \qquad (6)$$
$$Pu^{4+} + 5OH^- \leftrightarrow Pu(OH)_5^-, \quad \log\beta=53.8[21], \qquad (7)$$
$$Pu^{4+} + 4OH^- + 2HCO_3^- \leftrightarrow Pu(OH)_2(CO_3)_2^{2-} + 2H_2O, \quad \log\beta=54.15[22]. \qquad (8)$$

The solubility of Pu then can be calculated as the sum of $[Pu^{4+}]$ and the concentrations of complexation legands. Using the equilibrium constants(K) by Rai[19] and the complex stability constants(β) by Nitsche[21] and Yamaguchi[22], the solubility of Pu under the present conditions were calculated. In the calculations the temperature was assumed to be 25°C, because the thermodynamic data can not be found at 90°C.

Table 8 lists the results of the calculations compared with the measured concentrations of Pu in the 1.8nm filtrates. The concentrations of other hydrolysis species are too small to be taken into account. A relatively good agreement is found between the calculated Pu solubilities and the measured Pu concentrations under both redox conditions. These results suggest that precipitation of $PuO_2 \cdot xH_2O(am)$ is controlling the leaching of soluble species of Pu under both redox conditions, and the dominant soluble species are $Pu(OH)_4^0$ and/or $Pu(OH)_2(CO_3)_2^{2-}$ under oxidizing

conditions and $Pu(OH)_4^0$ under reducing conditions. Although Pu(IV) is suggested to be the dominant oxidation state under both redox conditions in the present study, Pu(IV) may be reduced to Pu(III) for longer times, and the corrosion tests for longer times are necessary.

The present results suggest that the colloidal particles with size from 1.8nm to 450nm are dominant phase for Pu and Cm in the solutions under both redox conditions. In addition, the concentrations of the colloidal particles of Pu and Cm was relatively high even in the early stage of glass corrosion and almost saturated after 20days of corrosion time as shown in Fig.8, which tendency is the same as that for other glass constituents such as Si, Ca and Al. While, the concentrations of the soluble species of Pu and Cm($\leq$1.8nm) were very low in the early stage of glass corrosion and increased slowly with corrosion time. These results suggest that formation of the colloidal particles of Pu and Cm are closely related to the leaching behavior of other glass constituents. For Ca and Al, the concentrations in the 1.8nm filtrates were thirty or forty percent of magnitude lower than those in non-filtered solution as shown in Table 6, which suggests that colloidal particles of these elements are present in the solutions. Buck et al.[23] and Fortner et al.[24] showed that clay colloids such as smectite and zeolite are produced as a direct result of the alteration of waste glass itself(primary colloids), and they can sorb or incorporate actinides strongly. Therefore, the colloidal particles of Pu and Cm observed under both redox conditions are expected to be weakly crystalline clay colloids sorbing Pu and Cm which are produced as a direct result of the glass alteration. The future work needs investigation of physical and chemical properties of the collodal particles for the long-term.

2.4 Conclusion of Glass Waste Forms

For the long-term evaluation of waste glass performance under repository condition, leachability has studied from the standpoints of understanding of alteration layers, effects of groundwater and effects of redox condition using the radioactive or non-radioactive glass samples. The summary is as follows:

(1) Leaching tests were carried out for a simulated waste glass in deionized water at 90°C for up to 364 days. The alteration layer thickness increased linearly at a rate of 0.63 μm/day for the first 91 days, and thereafter it remained constant (about 60 μm) independent of time, which corresponds to the forward and final reactions, respectively. The final rate of the layer growth was estimated to be 0.003-0.03 μm/day. Although the apparent release of elements from the glass almost ceases after the 91-day leaching, the reactions in the layers, such as crystal growth, continue.

(2) Under somewhat reducing conditions, Fe dissolves easily into leachates, and hydrated silicate surface layer on the glass surface tends to dissolve more easily with Fe in reduced synthetic groundwater than in deionized water. In synthetic groundwater, cracks originally present on the glass tend to open and are observed as evidence of congruent glass corrosion. It is speculated that, in deep geologic disposal sites, congruent dissolution is more likely to occur in an reducing environment with a high SA/V-ratio.

(3) Static corrosion tests were performed on the simulated waste glass doped with Pu and Cm under both redox conditions. Redox conditions have no remarkable influence on the leaching behavior of Pu and Cm. Colloidal particles with the size from 1.8nm to 450nm are dominant phase for Pu and Cm in the solution under both redox conditions, and the colloidal particles are suggested to be primary colloids. Comparison of the experimental results with the calculated results suggests that precipitation of $PuO_2 \cdot xH_2O$(am) is controlling the leaching of soluble species of Pu under both redox conditions, and the dominant soluble species are $Pu(OH)_4^0$ and/or $Pu(OH)_2(CO_3)_2^{2-}$ under oxidizing conditions and $Pu(OH)_4^0$ under reducing conditions.

3. CERAMIC WASTE FORMS

3.1 Radiation Stability of Perovskite and Phase and Chemical Stabilities of Zr- and Al-Based Ceramics [25]

JAERI has developed ceramic waste forms, e.g. Synroc [26] and zirconia-based ceramics, for immobilization of the high-level radioactive wastes arising from reprocessing of spent fuel and the actinide-rich wastes arising from partitioning and transmutation processes. In the present works, α-decay damage of perovskite, which is one of Synroc's constituent phases, and properties of zirconia- and alumina-based ceramics are discussed from the standpoint of the stability of crystal phases.

In our previous studies on Synroc [27,28], effects of α-decay damage on Synroc were investigated. Micro-encapsulation by more durable phases could mask the effects of the deterioration of less durable ones, in particular perovskite. Therefore single phase material is useful for getting direct information on this point. At present, we can utilize only limited data about the effect of α-decay damage on perovskite [28,30].

In the research and development of other host materials for the actinide-rich wastes, yttria-stabilized zirconia (YSZ), alumina compounds and YSZ-alumina composites have been selected based on the work from previous studies [31] and our preliminary examinations [32]. For the actinide-rich wastes, it is indispensable to immobilize the actinides in stable ceramic waste forms for a long time.

Experimental

α-decay damage of perovskite

The curium-doped perovskite, which had the following nominal composition:

$$Ca_{0.98919}(Cm,Pu)_{0.01081}Al_{0.01081}Ti_{0.98919}O_3$$

was made by hot-pressing at 1250 °C and 29 MPa for 2 hrs in a stream of N_2 gas. The curium source included 39 mol% of ^{244}Cm, and 56 mol% of ^{240}Pu that was a daughter nuclide of ^{244}Cm.

Density of a Cm-doped perovskite cylinder was periodically measured by the water displacement method. Half-disk specimens (2 cm in diameter, ~ 1 mm in thickness) that had accumulated doses of 1.6×10^{17}, 4.0×10^{17} and 8.3×10^{17} α-decays·g^{-1} were MCC-1 leach tested in pH ~ 2 buffer solution (0.05 M KCl + 0.013 M HCl) at 90°C for two months over four 7-day leach periods and a 28-day leach period. At the beginning of each leach period, the specimen was introduced to a new Teflon leach container with fresh leachant. After 2 cm^3 of leachate was withdrawn for pH measurement, 0.1 cm^3 of concentrated nitric acid was added to the remainder to minimize adsorption of Cm and precipitation of Ca. The leach containers with the leachate and sample support were subjected to NaI(Tl) scintillation spectrometry for the measurement of the total amount of ^{244}Cm leached [33]. The Ca and Ti concentration of leachates was measured by ICP-AES. As-leached and as-stored half-disk specimens were subjected to X-ray diffractometry.

Properties of zirconia- and alumina-based ceramics

Typical compositions of 3 types of ceramic waste forms are listed in Table 9. The stabilized zirconia is a powdered commercial product of fully stabilized zirconia. The alumina powder is a reagent grade α-alumina. The additions of Ce and Nd were designed to confirm the solid solution limits of Ce and/or Nd for each waste form. Each matrix and Ce and/or Nd oxides were directly weighed, and mixed using a ball mill. After pelletization and calcination, these pellets were crushed and re-mixed in the mill, and were uniaxially repressed at 36 MPa. Pellets of the YSZ were sintered in air at 1400 °C for 80 hrs and the others were heated in a stream of Ar-3 % H_2 gas at 1500°C for 25 hrs.

For the evaluation of crystallographic phase stability, crystalline phases formed in the samples were identified by X-ray diffractometry. Lattice parameters of fluorite-type structure formed in YSZ samples were determined by Nelson-Riley method [34]. The leach tests were carried out in deionized water for 114 days at 150 °C using powder samples of < 75 μm in size. The SA/V ratio was 1.8 x 10^4 - 1.2 x 10^5 m^{-1}. The powdered samples and the leachates were separated by the filtration using a millipore filter of 0.45 μm size. The Ce, Nd, Zr and Y concentrations of the leachates were determined by ICP-MS. Density of the samples was measured. The surface observation of the samples was carried out using a SEM-EDX.

Results and Discussions

α-decay damage of perovskite

Density

The average densities of the three cylinder samples were 4.083 $g \cdot cm^{-3}$ one month after hot pressing. As the amount of scatter of the three densities is < 0.05 % of the mean, the reproducibility of hot pressing is considered to be acceptable. Change in density of a Cm-doped perovskite sample is shown in Fig.9. The density changes are well fitted by a linear line. At a dose of 9 x 10^{17} α-decays$\cdot g^{-1}$, the fractional density decrease of the Cm-doped perovskite was 1.3 %.

Leaching

The change in the normalized Ca leach rate with time is shown in Fig.10. For the first 28 days, the Ca leach rate tends to rise with time. More damaged specimens gave a higher leach rate. In the final 28-day leaching run, the leachate was completely neutralized, and the Ca leach rate converged to a similar value. The Ca concentration of leachates that had pH > 5 was within 240 - 280 ppm. Therefore, the convergence of the Ca leach rate in the final 28-day leaching runs may be due to solubility limit of Ca in the neutralized solution. The Ti concentration in leachate was near the limit of detection. This is consistent with the replacement of perovskite by anatase on the surfaces of the as-leached Cm-doped perovskite specimens as detected by XRD (see section on surface alteration below).

The weight losses of half-disk specimens after two-month leach testing gave average leach rates of 1.7, 2.3 and 3.0 $g \cdot m^{-2} \cdot day^{-1}$ for the Cm-doped perovskite material that accumulated doses of 1.6 x 10^{17}, 4.0 x 10^{17}, and 8.3 x 10^{17} α-decays$\cdot g^{-1}$, respectively. If the dissolution of perovskite proceeds through the following reaction [35]:

$$CaTiO_3 + 2H^+ \longrightarrow Ca^{2+} + TiO_2\,(\text{anatase}) + H_2O \qquad (1),$$

the CaO weight loss of a specimen would correspond to its total weight loss because anatase (TiO_2) precipitated on specimen surfaces and contribution of the other minor elements would be negligible. A normalized leach rate derived from the CaO loss is similar to that from the total weight loss of Cm-doped perovskite. This similarity implies that the simple reaction mentioned above can be adopted as the dissolution mechanism of Cm-doped perovskite in the acidic solution at 90°C.

Figure 10 compares the leach rates of ^{244}Cm and Ca. For the first 28 days, the leach rates of ^{244}Cm and Ca tend to rise with time in a similar manner. In the final 28-day leaching run each of Ca and Cm leach rates converged to its constant value. The value for Cm leach rate is lower than that for Ca by a factor of > 20. This lower Cm leach rate in the final 28-day leaching runs may be due to little solubilization at pH values > ~ 7 [27]. It is possible that Cm and Pu oxides also precipitated on the Cm-doped specimens because an enrichment of Nd and Ce was observed on the nonradioactive specimens after leaching [36].

Surface Alteration

Figure 11 shows X-ray diffraction patterns from surfaces of as-leached and as-stored specimens that accumulated doses of 5.6×10^{17} and 5.2×10^{17} α-decays·g^{-1}, respectively. The as-stored specimen consisted only of the perovskite phase. On the other hand, the as-leached specimen contained anatase (TiO_2) in addition to the major phase, perovskite. Even though it is expected that higher Ca leach rate would leave larger amount of the Ti oxide on the Cm-doped specimens, the relative intensity of the anatase peaks from the as-leached surface of the Cm-doped perovskite was not so strong as that from the nonradioactive one [36]. This result is consistent with the fact that the as-leached surface of the Cm-doped perovskite was black as it was even after the leach testing. In Fig.11, the as-leached surface of Cm-doped perovskite contains a minor phase shown by a sign of "*", possibly (Cm, Pu)O_2 although all of the as-leached specimens did not show such clear appearance of this phase.

Properties of zirconia- and alumina-based ceramics

Phase Assemblages

For the YSZ samples, it was confirmed that the stabilized zirconia formed solid solutions with Ce or Nd and these solid solutions were stable in the wide content of $0 < Ce < 48.2$ or $0 < Nd < 19.4$ total cation in mol% as shown in Fig.12. The observed lattice parameters of fluorite-type structure in the YSZ samples increased linearly as in the following equations;

$$a_{Ce} = 0.51391 + 0.00029 \times [Ce] \quad (2),$$
$$a_{Nd} = 0.51385 + 0.00040 \times [Nd] \quad (3),$$

where [Ce] and [Nd] are cerium and neodymium concentration in mol% in stabilized zirconia solid solution, respectively. The Ce+Nd-bearing YSZ samples were stable in the content of $4.7 < (Ce, Nd) < 24.1$ in mol%, that is, a high rare earth content YSZ waste form, $Zr_{0.45}Y_{0.07}Ce_{0.24}Nd_{0.24}O_{1.83}$, could be produced by the sintering at 1400°C for 80 hrs in the air. The crystallographic similarity such as ionic radius, valence, electronegativity and crystal structure of each oxide among Zr, Y, Ce and Nd leads to the formation of the stable and high-containing solid solutions of the YSZ waste forms.

For the alumina compound waste forms, it was revealed that Ce was preferably stabilized in magnetoplumbite, $CeAl_{11}O_{18}$, by reacting with α-alumina in the Ce-bearing sample. On the other hand, Nd with α-alumina produced perovskite, $NdAlO_3$, and unreacted α-alumina. In the Ce+Nd-bearing sample, Ce-magnetoplumbite, Nd-perovskite and unreacted α-alumina were observed. From these results good crystallographic phase stability of the alumina compound waste forms was demonstrated. The formation of other phases with different crystal structure such as garnet-type, spinel-type and so on were not identified in the examination by XRD. This probably means that the formation of Nd-perovskite and the stabilization of Ce^{3+} in magnetoplumbite will proceed preferentially in the binary and ternary systems of Ce_2O_3 and/or Nd_2O_3-Al_2O_3 against the results of Mizuno et al. [37,38]. It seems that the difference of phase formation depends on the ionic radii of rare earth elements [39]. However the detailed SEM-EDX examination on each phase revealed that a little amount of Nd and Ce were detected in both magnetoplumbite and perovskite, that is, the formations of solid solution of Ce(Nd)-magnetoplumbite and Nd(Ce)-perovskite were observed.

For the YSZ-alumina composite waste forms, addition of Nd to the composite matrix brought about the formation of stabilized zirconia solid solution and perovskite, on the contrary, Ce addition produced stabilized zirconia solid solution and magnetoplumbite. In the Ce+Nd-bearing sample, the phases mentioned above were formed. Further the intimate mixing of α-alumina into stabilized zirconia did not lead

to a new phase formation. From these results it was revealed the YSZ-alumina composite waste forms possessed good phase stability, that is, the composite waste forms maintained the crystallographic phase stability of the YSZ and the alumina compound waste forms.

Chemical durability

Figure 13 shows the chemical durability of the YSZ samples. In the Ce-bearing YSZ samples Ce leach rates decreased with an increase in Ce contents, while Nd leach rates increased with an increase in Nd contents for the Nd-bearing samples. In the Ce+Nd-bearing samples Nd or Ce leach rates were an order of magnitude lower than those of the Nd- or Ce-bearing samples, respectively. At this stage, it is thought that this is due to the change of microstructure surrounding oxygen vacancies which were introduced into the YSZ waste forms by trivalent elements, Y and Nd, that is, the Ce-O or the Nd-O bond length surrounding the vacancies differs from the others far from the vacancies. On the other hand all values of chemical durability were below 10^{-6} $g \cdot m^{-2} \cdot day^{-1}$, lower remarkably than those of currently investigated borosilicate glasses because of high bonding energy between cations and oxygens in the YSZ waste forms. As mentioned, excellent chemical durability of the YSZ waste forms has been demonstrated.

Figure 14 also shows a summary of chemical durability of 3 types of the ceramic waste forms containing about 10 mol% of the Ce and Nd in deionized waste at 150°C. For the alumina compound samples chemical durability of each element was below 10^{-4} $g \cdot m^{-2} \cdot day^{-1}$, and these values were very lower than those of currently investigated borosilicate waste glasses. However, these values were more than two order of magnitudes higher than those of the YSZ samples, that is, chemical durability of the alumina compound samples was inferior to that of the YSZ samples.

For the YSZ-alumina composite samples, very low Ce leach rates in the Ce-bearing samples are also illustrated in Fig.14. This results means that Ce-magnetoplumbite as well as stabilized zirconia solid solution possess excellent chemical durability. Relatively high leach rates of Ce and Nd in the Nd- and the Ce+Nd-bearing samples of the alumina compound and the YSZ-alumina composite waste forms are thought to be caused by relatively poor chemical durability of perovskite, that is, chemical durabilities of stabilized zirconia solid solution and magnetoplumbite are superior to that of perovskite.

Density

The SEM-EDX observation showed that grain boundary segregation was not observed and each element was distributed homogeneously in the YSZ samples. The YSZ formed grains with a polyhedral shape which is due to isotropic grain growth based on cubic system of stabilized zirconia solid solution. The average grain size of a YSZ sample was 8.7 μm in diameter after the sintering at 1400°C in the air. This marked grain growth is caused by the fine particle size of the commercial powder of about 0.3 μm in diameter. Further, the isotropic and marked grain growth led to highly dense pellets with a relative density of 96.7 % .

For the alumina compound waste forms, the apparent densities of sintered pellet samples are listed in Table 10, which also shows the content of the phases. Densities of the alumina waste forms tended to decrease with an increase in the content of magnetoplumbite. From the results of SEM observation, the grain shape of magnetoplumbite was polygonal platelike. This anisotropic grain growth is due to the hexagonal system of this phase, and leads to the decrease in density as shown in Table 10. In order to produce a highly dense alumina compound waste form it seems important to suppress the formation of magnetoplumbite as far as possible.

3.2 Conclusion of Ceramic Waste Forms

α-decay damage of perovskite

Curium-doped perovskite samples were prepared in order to investigate the α-decay damage effects on the density and leaching behavior of perovskite. Change in density of Cm-doped perovskite reached 1.3 % at a dose of 9 x 10^{17} α-decays·g^{-1}. The rate of the density change was slightly larger in the present perovskite material than in Cm-doped Synrocs reported previously. Half-disk perovskite specimens, which had accumulated doses of 1.6 x 10^{17}, 4.0 x 10^{17} and 8.3 x 10^{17} α-decays·g^{-1}, were leach tested in pH~2 buffer solution at 90°C in a manner of MCC-1. The leach rate of perovskite, which was derived from weight losses after two-month leaching, was 1.7, 2.3 and 3.0 g·m^{-2}·day^{-1}. These high leach rate caused a significant increase in pH in the later stage of the leaching runs. For the first 28 days, the Ca and Cm leach rates at the three different doses increased with leach time. More damaged specimens gave higher leach rates. In the final 28-day leaching run, both Ca and Cm leach rates at three different doses converged on each lower value although the Cm leach rate was lower than the Ca leach rate by a factor of > 20. X-ray diffractometry on the as-leached surfaces of Cm-doped perovskite showed the clear appearance of anatase (TiO_2) reflections together with the major phase, perovskite.

Properties of zirconia- and alumina-based ceramics

The yttria-stabilized zirconia waste form was stable crystallographically over a wide range of Ce and/or Nd contents and it had excellent chemical durability. A highly dense pellet of the YSZ waste form could be obtained by the isotropic and marked grain growth. The alumina compound waste form consisted of two or three phases (α-alumina, magnetoplumbite and/or perovskite) with good phase stability. However, the chemical durability of the alumina compound waste form was relatively low possibly because of the presence of perovskite. Though the phase stability of the YSZ-alumina composite waste form was also good, it was inferior in chemical durability to the YSZ waste form possibly also due to the formation of perovskite. In conclusion, the YSZ is, on the whole, superior to the alumina compound and the YSZ-alumina composite as a waste form for the actinide-rich waste.

4. FUTURE WORKS

At JAERI the safety evaluation studies of waste forms and engineered barrier materials are in progress along the following three items.

1. The long-term corrosion of nuclear waste glasses is a key factor for the safety assessment of nuclear waste disposal. Therefore, the geochemical models for the predictions of long-term corrosion will be validated by various methods such as leaching experiments of actinide-doped waste glass, simulated and/or actual waste glass, natural analogues, and so on.
2. The capability and feasibility will be evaluated for titanate or zirconia based ceramic forms for the high-level radioactive waste.
3. Corrosion behavior of canister and overpack materials under disposal conditions will be studied for the long-term assessment of their durability.

REFERENCES

[1] T. Banba, T. Murakami, and H. Isobe, in *Scientific Basis for Nuclear Waste Management XIII*, edited by V.M. Oversby and P.W. Brown (Materials Research Society, Pittsburgh, 1990), p.363.

[2] R.C. Ewing and M.J. Jercinovic, in *Scientific Basis for Nuclear Waste Management X*, edited by J.K. Bates and W.B. Seefeldt (Materials Research Society, Pittsburgh, 1987), p.67.
[3] T. Murakami, T. Banba, M.J. Jercinovic and R.C. Ewing, in *Scientific Basis for Nuclear Waste Management XII*, edited by W. Lutze and R.C. Ewing (Materials Research Society, Pittsburgh, 1989), p.65.
[4] Materials Characterization Center, *Nuclear Waste Materials Handbook*, DOE/TIC-11400 (1981).
[5] B. Grambow, M.J. Jercinovic, R.C. Ewing and C.D. Byers, in *Scientific Basis for Nuclear Waste Management IX*, edited by L.O. Werme (Materials Research Society, Pittsburgh, 1986), p.263.
[6] B. Grambow, in *Scientific Basis for Nuclear Waste Management VIII*, edited by C.M. Jantzen, J.A. Stone and R.C. Ewing (Materials Research Society, Pittsburgh, 1985), p.15.
[7] Zhihong Zhou and W.S. Fyfe, in *Scientific Basis for Nuclear Waste Management XI*, edited by M.J. Apted and R.E. Westerman (Materials Research Society, Pittsburgh, 1988), p.725.
[8] A.B. Harker and J.F. Flintoff, Nucl. Technol., 76, 263 (1987).
[9] W.G. Melson and G. Thompson, Geol. Soc. America Bull., 84, 703 (1973).
[10] H. Kamizono, J. Nucl. Mater., 172, 319 (1990).
[11] H. Kamizono, J. Mater. Sci. Lett., 9, 841 (1990).
[12] Y.Inagaki *et al.*, Mat.Res.Soc.Proc., (in press) (1997).
[13] Y.Inagaki, A.Ogata, H.Furuya, K.Idemitsu, T.Banba and T.Maeda, Mat.Res.Soc.Proc.Vol.412, 257 (1996).
[14] E.Y.Vernaz and N.Gordon, Mat.Res.Soc.Proc.Vol.257, 37 (1992).
[15] L.Wang and P.Van Iseghem, Mat.Res.Soc.Proc.Vol.294, 155 (1993).
[16] J.I.Kim, W.Treiber, Ch.Lierse and P.Offermann, Mat.Res.Soc.Proc.Vol.44, 359 (1985).
[17] D.Rai, R.J.Serne and D.A.Moore, Soil Sci.Soc.Am.J., 44, 490 (1980).
[18] B.Allard, *The Solubility of Actinides in Neutral and Basic Solutions in Actinides in Perspective*, edited by N.M.Edelstein(Pergamon Press, Oxford,1982).
[19] D.Rai, Radiochimica Acta, 35, 97 (1984).
[20] J.I.Kim and B.Kanellakopulos, Radiochimica Acta, 48, 145 (1989).
[21] H.Nitsche, Mat.Res.Soc.Proc.Vol.212, 517 (1991).
[22] T.Yamaguchi, Y.Sakamoto, T.Ohnuki, Radiochimica Acta, 66/67, 9 (1994).
[23] E.C.Buck, J.K.Bates *et al.*, Mat.Res.Soc.Proc.Vol.294, 199 (1993).
[24] J.A.Fortner and J.K.Bates, Mat.Res.Soc.Proc.Vol.412, 205 (1996).
[25] K.Kuramoto, H.Mitamura, T.Banba, S.Muraoka, Progress in Nuclear Energy, (in press) (1997).
[26] A.E.Ringwood *et al.*, *Radioactive Waste Forms for The Future* (W.Lutze, and R.C.Ewing, ed.), pp. 233-334. Elsevier Science Publishers, New York (1988).
[27] H.Mitamura *et al.*, J.Am.Ceram.Soc., 75, 392 (1992).
[28] H.Mitamura *et al.*, J.Am.Ceram.Soc., 77, 2255 (1994).
[29] E.Vernaz *et al.*, *Long-Term Stability of High-Level Waste Forms*, CEA-CONF-10429 (1990).
[30] W.Sinclair and A.E.Ringwood, Geochem.J., 15, 229 (1981).
[31] H.Kamizono *et al.*, J.Am.Ceram.Soc., 74, 863 (1991).
[32] I.Hayakawa and H.Kamizono, J.Nucl.Sci.Technol., 30, 673 (1993).
[33] H.Mitamura *et al.*, Appl.Radiat.Isot., 41, 839 (1990).
[34] C.Whiston, *X-Ray Method* , edited by C.Whiston, pp. 132-164. John Wiley & Sons, New York (1985).
[35] D.K.Pham *et al.*, in *Scientific Basis for Nuclear Waste Management XII* , edited by W.Lutze and R.C.Ewing (Materials Research Society, Pittsburgh, 1989), p.231.
[36] H.Mitamura *et al.*, in *Scientific Basis for Nuclear Waste Management XVIII* , edited by T.Murakami and R.C.Ewing (Materials Research Society, Pittsburgh, 1995), p.1405.
[37] M.Mizuno *et al.*, Yogyo Kyokaishi., 83, 90 (1975).

[38] M.Mizuno *et al.*, Yogyo Kyokaishi., 85, 90 (1977).
[39] N.Iyi *et al.*, J. Solid State Chem., 83, 8 (1989).

Table 1 Bulk composition of the borosilicate waste glass.

Component	wt %	Component	wt %
Additives		FP oxides	
SiO_2	48.49	CoO	0.12[c]
B_2O_3	18.58	NiO	0.33[d]
Al_2O_3	2.00	TeO_2	0.23
Li_2O	1.87	Cs_2O	0.98
Na_2O	11.30	BaO	0.63
CaO	1.87	La_2O_3	0.51
Fe_2O_3	3.55[a]	CeO_2	1.42[e]
ZrO_2	2.87[b]	Pr_6O_{11}	0.50
		Nd_2O_3	1.65
FP oxides		Sm_2O_3	0.33
Rb_2O	0.12	Ag_2O	0.03
SrO	0.34	CdO	0.03
Y_2O_3	0.20	SnO_2	0.02
MoO_3	1.74	Sb_2O_3	0.004
MnO_2	0.26	Gd_2O_3	0.04

[a] Partly simulates RuO_2. [b] Partly includes ZrO_2 as FP.
[c] Simulates Rh_2O_3. [d] Simulates PdO.
[e] Partly simulates actinides.

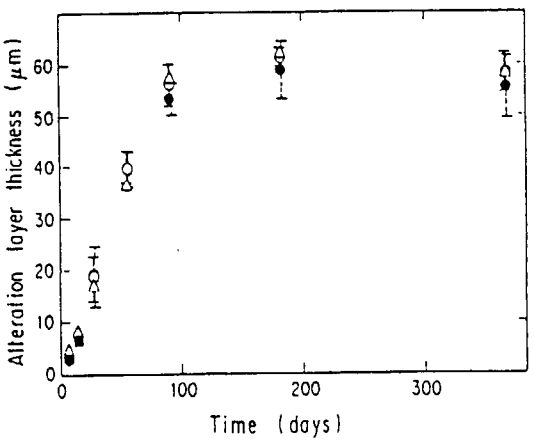

Fig. 1 Graph of the thickness of alteration layer as a function of leaching time under the MCC-1 conditions at 90°C. The open and solid circles indicate thicknesses averages for the ethanol-immersed and air-dried layers, respectively. The error bars represent the variabilities of the layer thicknesses. The triangles indicate layer thicknesses calculated from the amounts of B released in leachates.

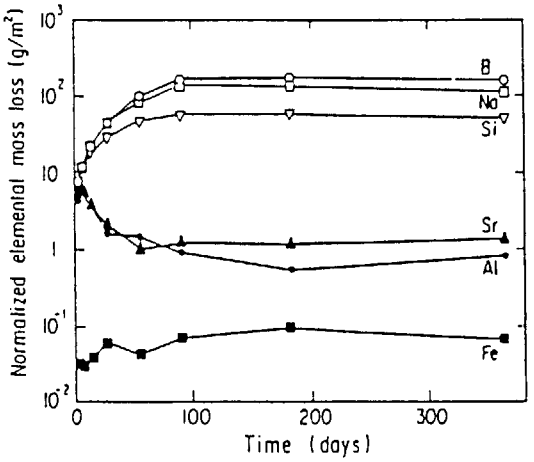

Fig. 2 Normalized elemental mass losses of selected elements of the nuclear waste glass in deionized water with time.

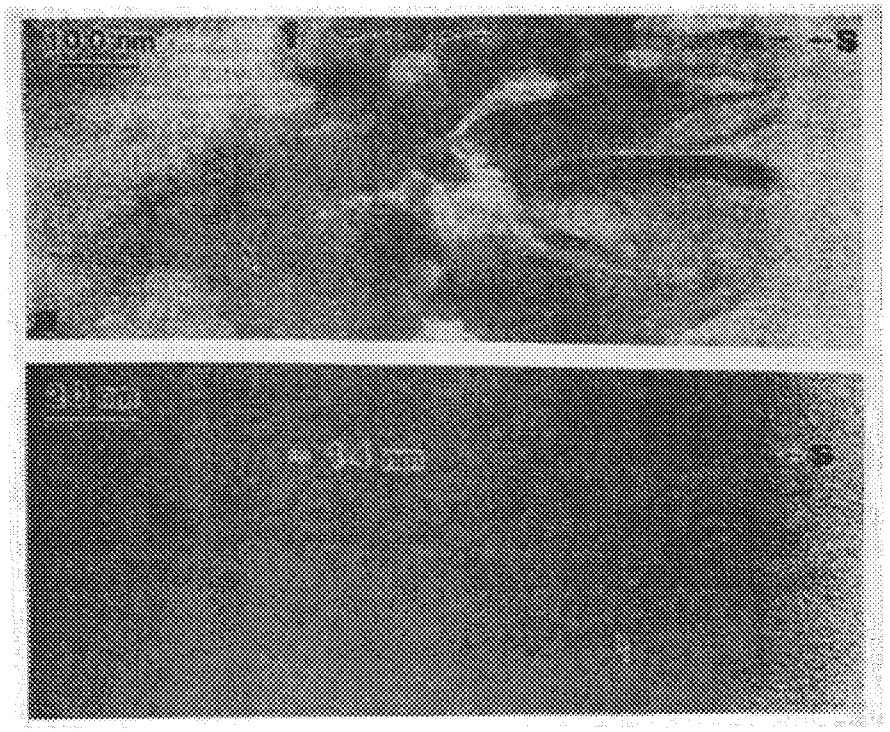

Fig. 3 TEM micrographs of the borosilicate glass layer. (a) Part of the layer in the 91-day experiment. 1 denotes the mottled phase in the layer [3] ; 2, the zone of the fibers formed on the layer; 3, the zone of the new crystals (possibly smectite); S, solution which is now filled with resin. The zones are parallel to the glass. The arrow indicates an example of the fibers in the mottled phase. (b) Part of the zone of the new crystals in the 364-day experiment. S shows the layer/solution interface. The d-spacings of the new crystals are mostly 1.4nm. Note that the c-axis, which is normal to the fringes, is parallel to the layer/solution interface or normal to the possible direction of cation diffusion. The arrow indicates an example of edge dislocation.

Table 2 AEM analyses of the new crystal (possibly smectite), fiber and mottled phase in the 364-day experiment (mass fraction, %).

	Na_2O	Al_2O_3	SiO_2	ZrO_2	CaO	MoO_3	MnO_2	FeO	CoO	NiO	REO[a]
New crystal	1.0	4.8	59.2	0.0	0.4	0.5	4.2	0.8	7.6	21.6	0.0
Fiber	1.5	8.5	49.2	0.0	0.6	0.5	4.3	10.6	5.5	19.3	0.0
Mottled[b]	1.5	3.4	55.4	10.6	1.7	0.4	1.9	10.9	0.6	2.0	11.7

[a] Sum of La_2O_3, CeO, and Nd_2O_3.
[b] See reference 3 for explanation of "mottled".

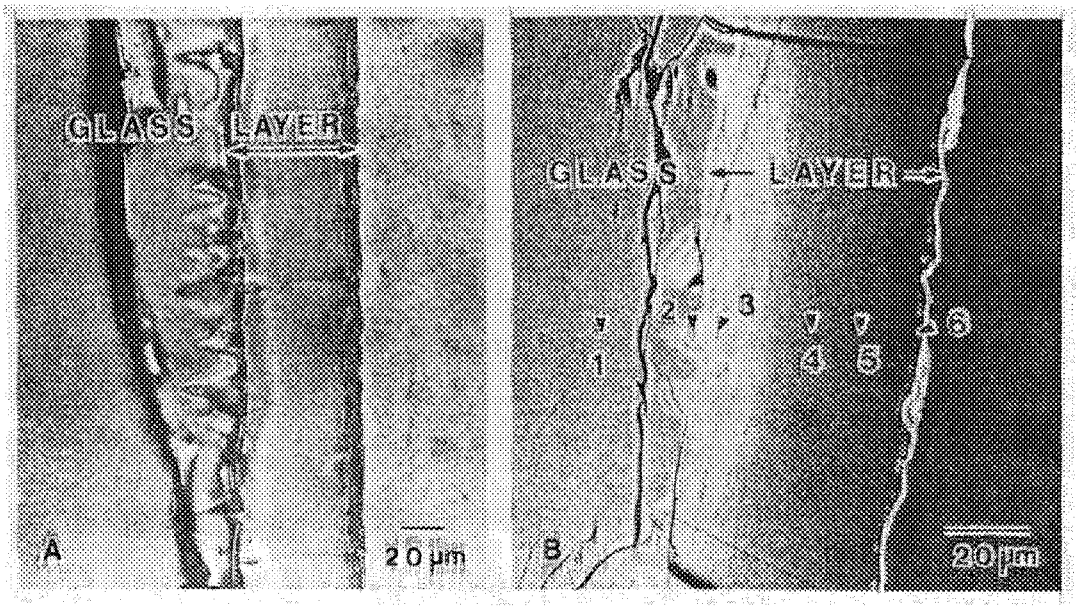

Fig. 4 Micrographs of the air-dried alteration layer in the 182-day experiment. (A) Optical view of the layer cross section showing cone-shaped pits. (B) SEM view (backscattered electron image) showing pits at the glass /layer interface. The locations of the six microprobe analyses are illustrated by the black arrowheads. The arabic numbers indicate the analytical points, corresponding to those in Table 3.

Table 3 Microprobe analyses (wt%)[a] of the glass and the alteration layer. The arabic numbers indicate the locations shown in Fig. 3B.

	Na_2O	Al_2O_3	SiO_2	CaO	MnO	FeO	Total
Bulk glass							
1	11.3	1.5	46.5	1.6	0.3	2.9	64.1
Layer							
2	2.2	2.5	50.4	5.4	0.4	3.8	64.7
3	1.5	2.5	51.1	4.2	0.3	4.2	63.8
4	1.4	3.1	42.9	2.2	-	3.9	53.5
5	1.7	2.8	37.0	2.1	0.4	3.7	47.7
6	-	1.5	29.3	1.6	0.7	3.6	36.7

[a] Obtained by Energy Dispersive X-ray (EDX) Analysis.

Table 4 Composition of synthetic groundwater

	Synthetic groundwater			
	No. 1	No. 2	No.3	No. 4
pH	7.7	7.7	7.7	7.7
Na (in mg/l) [a)]	26	26	26	26
Ca	120	120	–	–
Mg	108	108	108	–
HCO_3^-	Nearly saturated			
SO_4^{2-}	380	–	–	–

–: Not included.

[a)] The amount of each element in the synthetic groundwater is in the average concentration range of the respective element in the natural groundwater.

Table 5 The ratio of NL_{Fe}/NL_B in the leachates

Leach conditions	Synthetic groundwater				Deionized water
	No. 1	No. 2	No. 3	No. 4	
70°C, 28 days	0.35	0.36	0.66	0.24	0.0021
70°C, 49 days	0.13	0.24	0.20	0.51	0.0014
20°C, 1 year, not filtered	0.85	0.98	0.97	0.55	0.14
20°C, 1 year, filtered	1.02	0.82	1.01	0.59	0.16

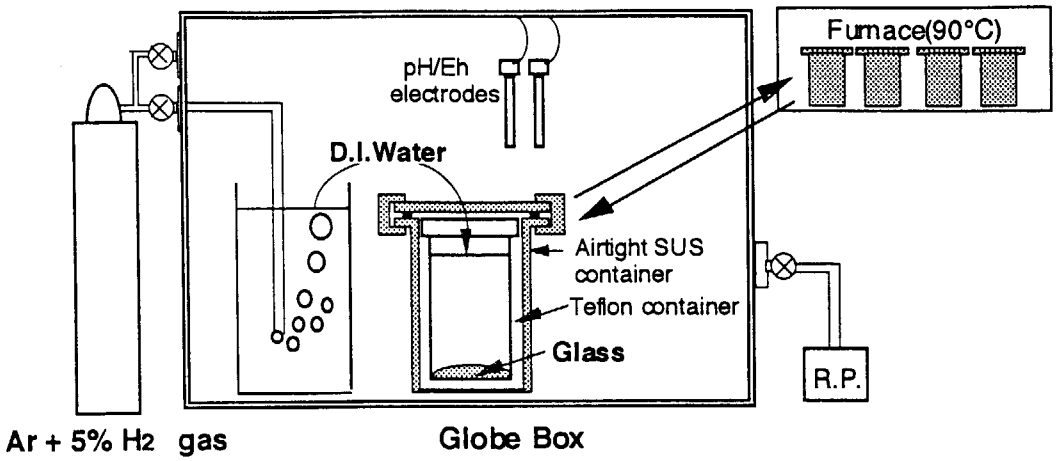

Fig.5 Schematic representative of corrosion tests under reducing conditions.

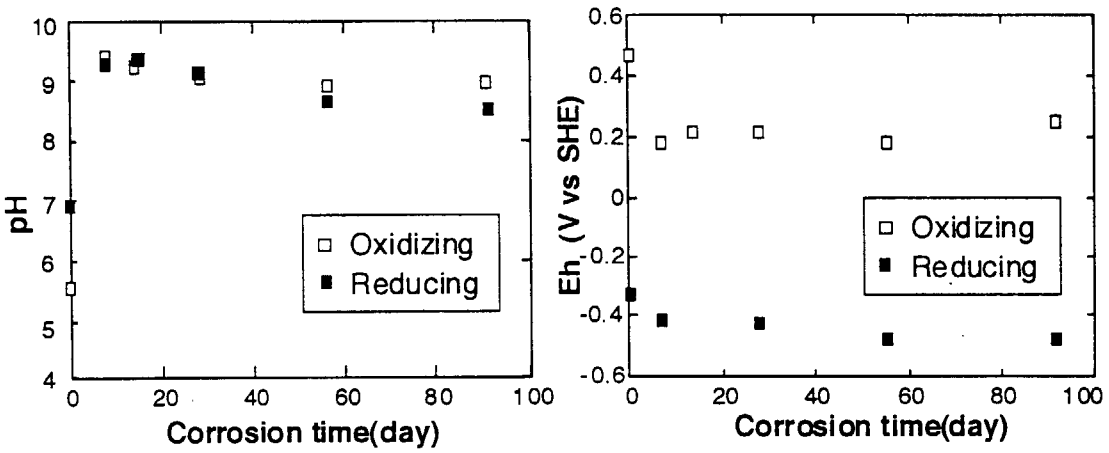

Fig.6 Solution pH and Eh as a function of corrosion time.

Table 6 Solution concentrations of major glass constituents.

Corrosion time[day]	Redox condition	Filtration	Solution concentration[ppm] Si	B	Li	Mo	Na	Ca	Al
7	Oxidizing	no-filtration	45.0	23.3	4.98	6.01	34.1	1.25	0.68
	Reducing		42.7	21.4	4.61	5.76	30.2	1.37	0.59
14	Oxidizing	no-filtration	56.5	35.2	7.57	8.88	49.8	1.31	0.64
	Reducing		53.4	32.6	6.84	8.63	46.1	1.38	0.55
28	Oxidizing	no-filtration	59.3	38.1	8.36	9.34	60.8	1.23	0.66
	Reducing		58.4	36.4	7.85	8.88	59.7	1.16	0.65
56	Oxidizing	no-filtration	67.9	52.7	11.0	11.5	75.8	0.74	0.76
	Reducing		64.9	49.5	10.4	8.68	72.2	1.49	0.72
92	Oxidizing	no-filtration	73.0	73.0	15.1	12.2	94.7	1.02	1.06
	Reducing		70.6	84.2	17.0	10.5	117.0	2.16	1.12
92	Oxidizing	1.8nm	72.7	70.0	14.8	12.0	93.8	0.62	0.73
	Reducing		63.0	75.0	16.0	6.68	104.2	1.72	0.70

Table 7 Solution concentrations of Pu and Cm.

Corrosion time[day]	Redox condition	Solution concentration[mol/l]					
		Pu			Cm		
		no-filtration	450nm	1.8nm	no-filtration	450nm	1.8nm
7	Oxidizing	4.0×10^{-8}	4.1×10^{-8}	2.4×10^{-9}	3.5×10^{-9}	3.1×10^{-9}	2.5×10^{-11}
	Reducing	7.6×10^{-8}	5.5×10^{-8}	2.3×10^{-9}	6.9×10^{-9}	6.4×10^{-9}	7.5×10^{-12}
14	Oxidizing	5.1×10^{-8}	3.2×10^{-8}	2.4×10^{-9}	4.8×10^{-9}	4.3×10^{-9}	3.1×10^{-11}
	Reducing	9.5×10^{-8}	1.1×10^{-7}	3.1×10^{-9}	8.6×10^{-9}	7.4×10^{-9}	2.2×10^{-11}
28	Oxidizing	9.8×10^{-8}	1.7×10^{-7}	--	4.8×10^{-9}	3.8×10^{-9}	--
	Reducing	1.3×10^{-7}	1.6×10^{-7}	1.5×10^{-8}	9.9×10^{-9}	7.8×10^{-9}	1.1×10^{-9}
56	Oxidizing	1.4×10^{-7}	1.1×10^{-7}	1.0×10^{-8}	1.2×10^{-8}	8.4×10^{-9}	2.7×10^{-10}
	Reducing	1.5×10^{-7}	1.2×10^{-7}	–	8.8×10^{-9}	7.9×10^{-9}	--
92	Oxidizing	2.5×10^{-7}	1.6×10^{-7}	1.5×10^{-8}	4.3×10^{-8}	9.7×10^{-9}	5.7×10^{-10}
	Reducing	2.3×10^{-7}	2.3×10^{-7}	2.2×10^{-8}	1.4×10^{-8}	1.2×10^{-8}	9.1×10^{-10}

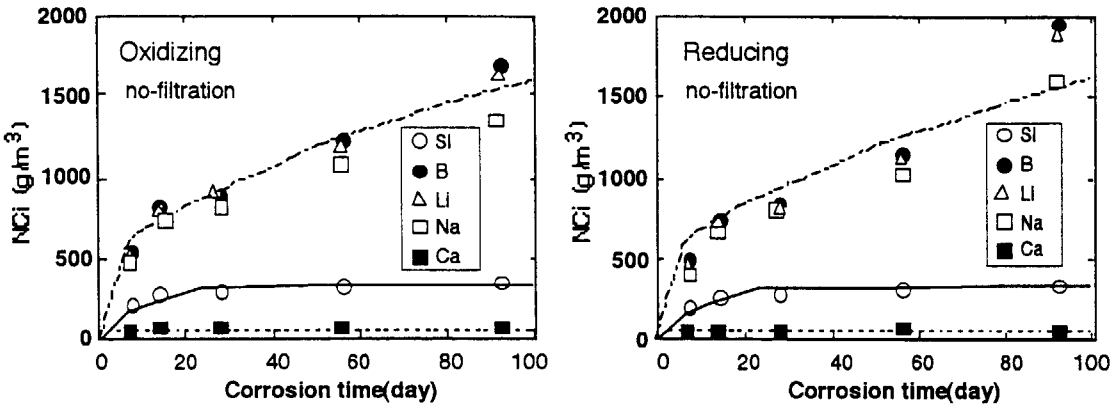

Fig.7 NC_i for major glass constituents under oxidizing and reducing conditions.

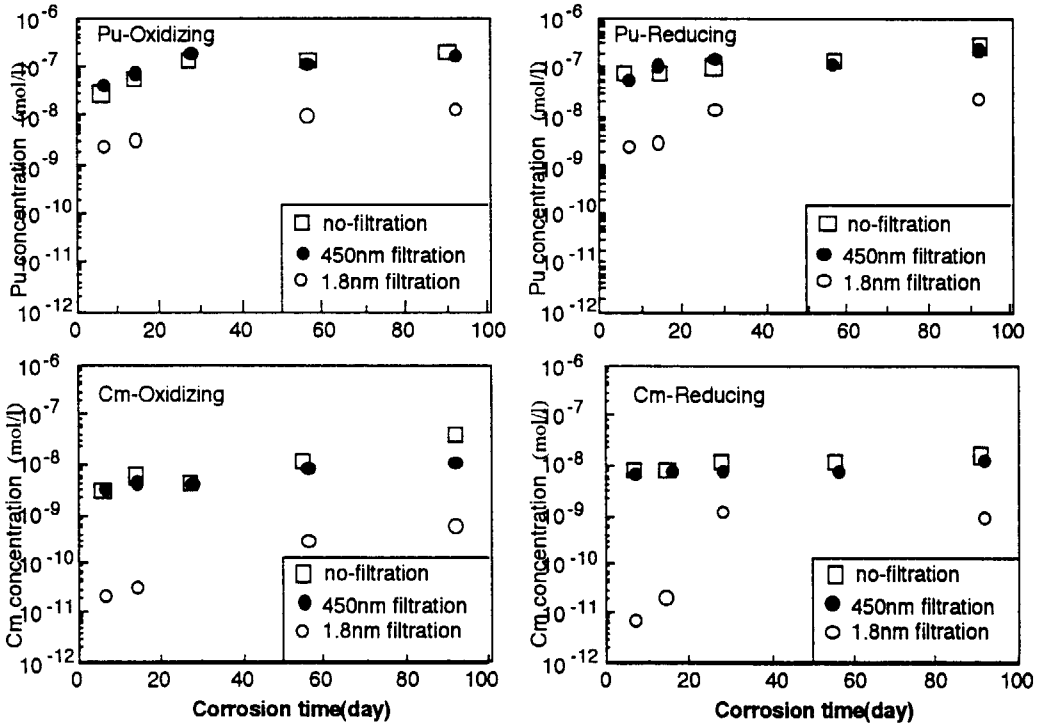

Fig.8 Solution concentrations of Pu and Cm under oxidizing and reducing conditions.

Table 8 Solubility of Pu(IV) calculated by using the equilibrium constants by Rai[19] and the complex stability constants by Nitsche[21] and Yamaguchi[22] compared with the measured concentrations.

Oxidizing conditions (pH=8.8, Eh=+0.25 V vs SHE, $P_{CO2}=10^{-3.5}$)	
Calculated solubility of Pu(IV) ($25℃$, $PuO_2 \cdot xH_2O$(am) is the solubility control. phase)	Measured Pu concentration ($90℃$, 92days, 1.8nm filtration)
$[Pu(OH)_4^0] = 2.2\times10^{-8}M$ $[Pu(OH)_5^-] = 5.0\times10^{-9}M$ $[Pu(OH)_2(CO_3)_2^{2-}] = 1.8\times10^{-8}M$ $[Pu(IV)]_{total} = 4.5\times10^{-8}M$	$[Pu]_{total} = 1.5\times10^{-8}M$
Reducing conditions (pH=8.6, Eh=-0.45 V vs SHE, $P_{CO2}\approx0$)	
Calculated solubility of Pu(IV) ($25℃$, $PuO_2 \cdot xH_2O$(am) is the solubility control. phase)	Measured Pu concentration ($90℃$, 92days, 1.8nm filtration)
$[Pu(OH)_4^0] = 2.2\times10^{-8}M$ $[Pu(OH)_5^-] = 3.0\times10^{-9}M$ $[Pu(IV)]_{total} = 2.5\times10^{-8}M$	$[Pu]_{total} = 2.2\times10^{-8}M$

Table 9 Compositions of ceramic waste forms in mol%*

Sample	Yttria-stabilized zirconia (YSZ) waste forms								Alumina compound waste forms			YSZ-alumina composite waste forms					
	YSZ	YC-10	YC-50	YN-10	YN-20	YCN-10	YCN-20	YCN-50	AC-8	ACN-8	AN-8	AZ_3-N	A_3Z-N	AZ_3-CN	A_3Z-CN	AZ_3-C	A_3Z-C
Matrix																	
ZrO_2	85.7	76.0	44.4	77.4	69.1	77.7	69.6	44.4	----	----	----	43.9	11.0	45.6	11.3	47.5	11.6
$YO_{1.5}$	14.3	12.7	7.4	12.9	11.5	12.9	11.6	7.4	----	----	----	7.3	1.8	7.6	1.9	7.9	1.9
$AlO_{1.5}$	----	----	----	----	----	----	----	----	91.6	91.6	91.6	33.8	75.9	35.1	78.1	36.5	80.5
TRU simulant																	
CeO_2	----	11.3	48.2	----	----	4.7	9.4	24.1	8.4	4.2	----	----	----	3.9	2.9	8.1	6.0
$NdO_{1.5}$	----	----	----	9.7	19.4	4.7	9.4	24.1	----	4.2	8.4	15.0	11.3	7.8	5.8	----	----

*: Compositions of each constituent indicate the contents of each cation to total cations in mol%.

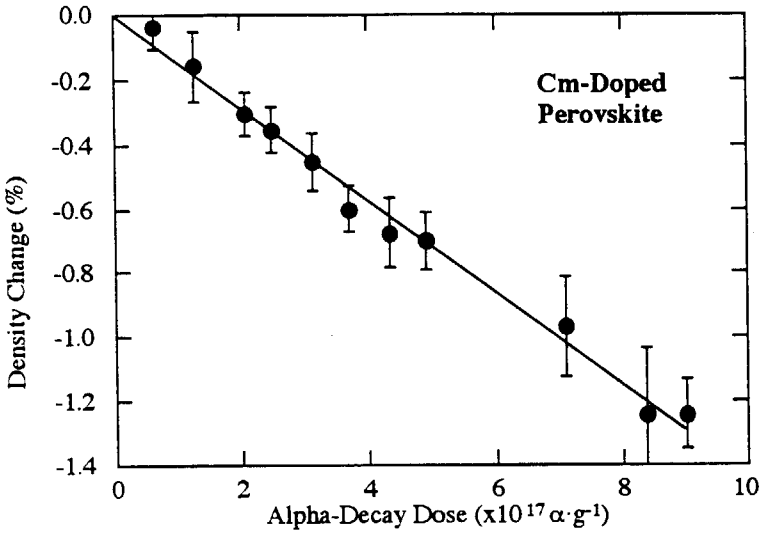

Fig.9 Density change of Cm-doped perovskite versus α-decay dose.

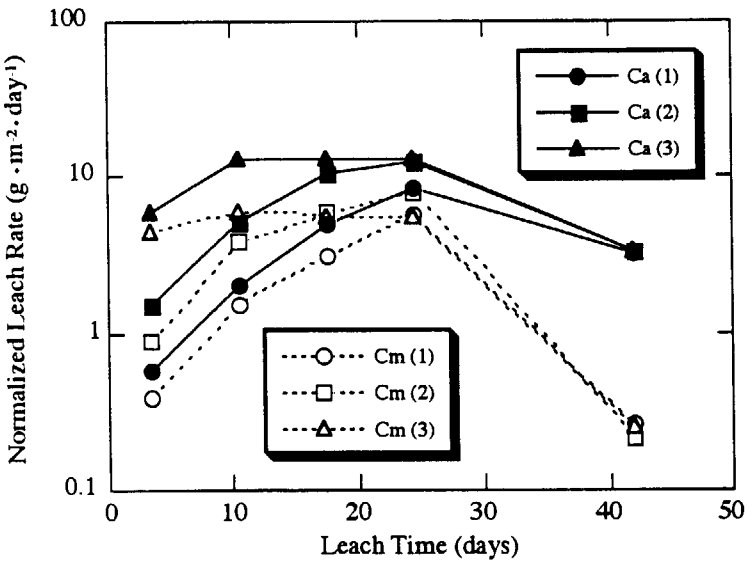

Fig.10 Change in normalized Ca and Cm leach rates with time. The specimens accumulated doses of (1) 1.6 x 10^{17}, (2) 4.0 x 10^{17} and (3) 8.3 x 10^{17} α-decays·g^{-1}.

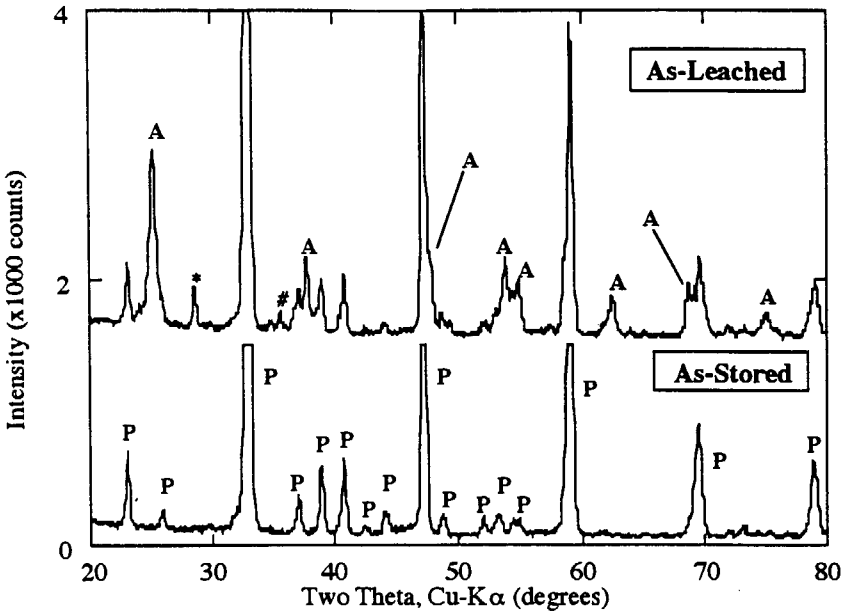

Fig.11 X-ray diffraction patterns from as-leached and as-stored surfaces of Cm-doped perovskite. The signs of A, P, * , and # stand for anatase (TiO_2), perovskite, $(Cm, Pu)O_2$, and unidentified peaks, respectively.

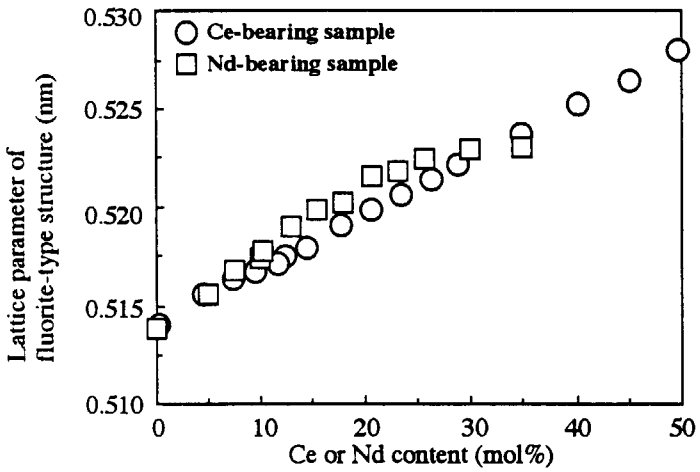

Fig.12 Lattice parameter variations of yttria-stabilized zirconia (YSZ) waste forms formed by the addition of Ce or Nd.

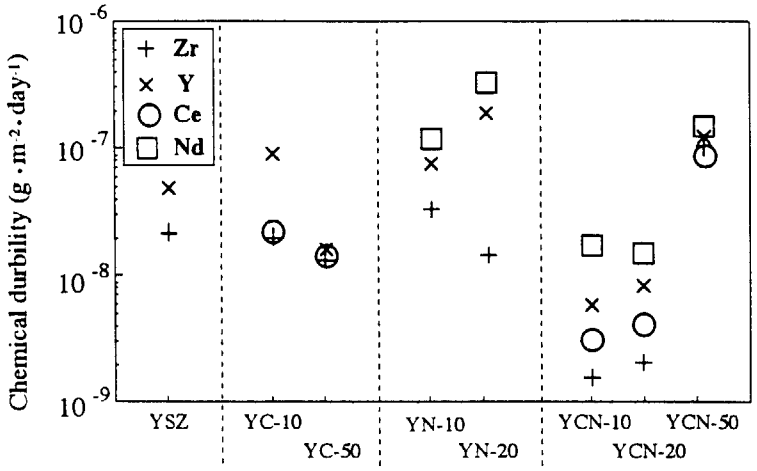

Fig.13 Chemical durability of powdered yttria-stabilized zirconia (YSZ) waste forms in deionized water at 150 °C for 114 days.

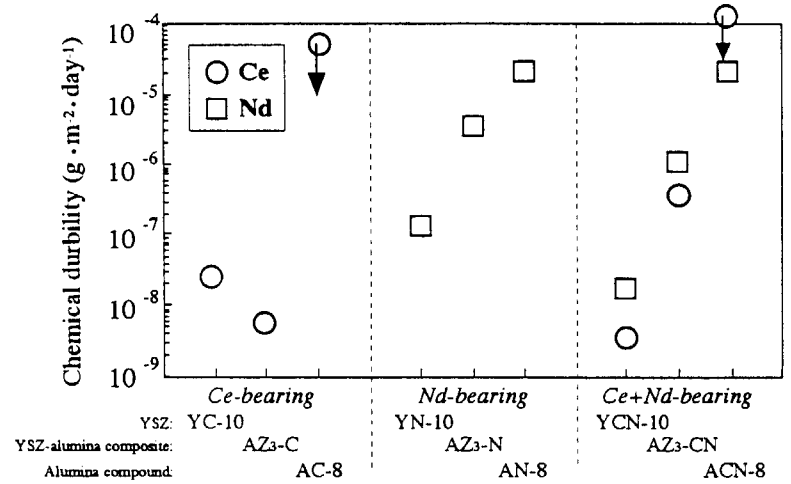

Fig.14 Chemical durability of yttria-stabilized zirconia (YSZ), alumina compound and YSZ-alumina composite waste forms containing about 10 mol% of Ce and/or Nd in deionized water at 150°C for 114 days.

Leach rates marked by circles with an arrow were measured by an inductively coupled plasma atomic emission spectrometry and indicate detection limits of Ce.

Table 10 Phase content and density of alumina compound waste forms

Property	AC-8	ACN-8	AN-8
Phase content (wt%)			
α-alumina	0.0	34.6	45.2
Perovskite	0.0	34.2	54.8
Magnetoplumbite	100.0	31.2	0.0
Density ($g \cdot cm^{-3}$)	2.21	3.02	3.41

This is a blank page.

国際単位系 (SI) と換算表

表 1　SI 基本単位および補助単位

量	名称	記号
長さ	メートル	m
質量	キログラム	kg
時間	秒	s
電流	アンペア	A
熱力学温度	ケルビン	K
物質量	モル	mol
光度	カンデラ	cd
平面角	ラジアン	rad
立体角	ステラジアン	sr

表 2　SI と併用される単位

名称	記号
分，時，日	min，h，d
度，分，秒	°，′，″
リットル	l，L
トン	t
電子ボルト	eV
原子質量単位	u

1 eV = 1.60218 × 10^{-19} J

1 u = 1.66054 × 10^{-27} kg

表 5　SI 接頭語

倍数	接頭語	記号
10^{18}	エクサ	E
10^{15}	ペタ	P
10^{12}	テラ	T
10^{9}	ギガ	G
10^{6}	メガ	M
10^{3}	キロ	k
10^{2}	ヘクト	h
10^{1}	デカ	da
10^{-1}	デシ	d
10^{-2}	センチ	c
10^{-3}	ミリ	m
10^{-6}	マイクロ	μ
10^{-9}	ナノ	n
10^{-12}	ピコ	p
10^{-15}	フェムト	f
10^{-18}	アト	a

表 3　固有の名称をもつ SI 組立単位

量	名称	記号	他の SI 単位による表現
周波数	ヘルツ	Hz	s^{-1}
力	ニュートン	N	m·kg/s^2
圧力，応力	パスカル	Pa	N/m^2
エネルギー，仕事，熱量	ジュール	J	N·m
工率，放射束	ワット	W	J/s
電気量，電荷	クーロン	C	A·s
電位，電圧，起電力	ボルト	V	W/A
静電容量	ファラド	F	C/V
電気抵抗	オーム	Ω	V/A
コンダクタンス	ジーメンス	S	A/V
磁束	ウェーバ	Wb	V·s
磁束密度	テスラ	T	Wb/m^2
インダクタンス	ヘンリー	H	Wb/A
セルシウス温度	セルシウス度	℃	
光束	ルーメン	lm	cd·sr
照度	ルクス	lx	lm/m^2
放射能	ベクレル	Bq	s^{-1}
吸収線量	グレイ	Gy	J/kg
線量当量	シーベルト	Sv	J/kg

表 4　SI と共に暫定的に維持される単位

名称	記号
オングストローム	Å
バーン	b
バール	bar
ガル	Gal
キュリー	Ci
レントゲン	R
ラド	rad
レム	rem

1 Å = 0.1 nm = 10^{-10} m

1 b = 100 fm^2 = 10^{-28} m^2

1 bar = 0.1 MPa = 10^5 Pa

1 Gal = 1 cm/s^2 = 10^{-2} m/s^2

1 Ci = 3.7 × 10^{10} Bq

1 R = 2.58 × 10^{-4} C/kg

1 rad = 1 cGy = 10^{-2} Gy

1 rem = 1 cSv = 10^{-2} Sv

（注）

1. 表 1 − 5 は「国際単位系」第 5 版，国際度量衡局 1985 年刊行による。ただし，1 eV および 1 u の値は CODATA の 1986 年推奨値によった。
2. 表 4 には海里，ノット，アール，ヘクタールも含まれているが日常の単位なのでここでは省略した。
3. bar は，JIS では流体の圧力を表わす場合に限り表 2 のカテゴリーに分類されている。
4. EC 閣僚理事会指令では bar，barn および「血圧の単位」mmHg を表 2 のカテゴリーに入れている。

換　算　表

力	N(=10^5 dyn)	kgf	lbf
	1	0.101972	0.224809
	9.80665	1	2.20462
	4.44822	0.453592	1

粘　度　1 Pa·s(N·s/m^2) = 10 P(ポアズ)(g/(cm·s))

動粘度　1 m^2/s = 10^4 St(ストークス)(cm^2/s)

圧力	MPa(=10 bar)	kgf/cm^2	atm	mmHg(Torr)	lbf/in^2(psi)
	1	10.1972	9.86923	7.50062 × 10^3	145.038
	0.0980665	1	0.967841	735.559	14.2233
	0.101325	1.03323	1	760	14.6959
	1.33322 × 10^{-4}	1.35951 × 10^{-3}	1.31579 × 10^{-3}	1	1.93368 × 10^{-2}
	6.89476 × 10^{-3}	7.03070 × 10^{-2}	6.80460 × 10^{-2}	51.7149	1

エネルギー・仕事・熱量	J(=10^7 erg)	kgf·m	kW·h	cal(計量法)	Btu	ft·lbf	eV
	1	0.101972	2.77778 × 10^{-7}	0.238889	9.47813 × 10^{-4}	0.737562	6.24150 × 10^{18}
	9.80665	1	2.72407 × 10^{-6}	2.34270	9.29487 × 10^{-3}	7.23301	6.12082 × 10^{19}
	3.6 × 10^6	3.67098 × 10^5	1	8.59999 × 10^5	3412.13	2.65522 × 10^6	2.24694 × 10^{25}
	4.18605	0.426858	1.16279 × 10^{-6}	1	3.96759 × 10^{-3}	3.08747	2.61272 × 10^{19}
	1055.06	107.586	2.93072 × 10^{-4}	252.042	1	778.172	6.58515 × 10^{21}
	1.35582	0.138255	3.76616 × 10^{-7}	0.323890	1.28506 × 10^{-3}	1	8.46233 × 10^{18}
	1.60218 × 10^{-19}	1.63377 × 10^{-20}	4.45050 × 10^{-26}	3.82743 × 10^{-20}	1.51857 × 10^{-22}	1.18171 × 10^{-19}	1

1 cal = 4.18605 J (計量法)

= 4.184 J (熱化学)

= 4.1855 J (15 °C)

= 4.1868 J (国際蒸気表)

仕事率　1 PS (仏馬力)

= 75 kgf·m/s

= 735.499 W

放射能	Bq	Ci
	1	2.70270 × 10^{-11}
	3.7 × 10^{10}	1

吸収線量	Gy	rad
	1	100
	0.01	1

照射線量	C/kg	R
	1	3876
	2.58 × 10^{-4}	1

線量当量	Sv	rem
	1	100
	0.01	1

（86 年 12 月 26 日現在）

STUDIES OF HIGH-LEVEL WASTE FORM PERFORMANCE AT JAPAN ATOMIC ENERGY RESEARCH INSTITUTE